Microelectronic Engineering 267–268 (2023) 111912

Contents lists available at ScienceDirect

Microelectronic Engineering

journal homepage: www.elsevier.com/locate/mee

Capacitive immunosensor for COVID-19 diagnosis

Isabella Sampaio [*,1], Nayla Naomi Kusimoto Takeuti [1], Beatriz Gusson, Thales Rafael Machado, Valtencir Zucolotto

GNano – Nanomedicine and Nanotoxicology Group, São Carlos Institute of Physics, University of São Paulo CP 369, 13560-970 São Carlos, SP, Brazil

ARTICLE INFO

Keywords:
Capacitive biosensor
COVID-19 diagnosis
Spike protein detection
Immunosensor

ABSTRACT

COVID-19 has spread worldwide and early detection has been the key to controlling its propagation and preventing severe cases. However, diagnostic devices must be developed using different strategies to avoid a shortage of supplies needed for tests' fabrication caused by their large demand in pandemic situations. Furthermore, some tropical and subtropical countries are also facing epidemics of Dengue and Zika, viruses with similar symptoms in early stages and cross-reactivity in serological tests. Herein, we reported a qualitative immunosensor based on capacitive detection of spike proteins of the severe acute respiratory syndrome coronavirus 2 (SARS-CoV-2), the causative agent of COVID-19. The sensor device exhibited a good signal-to-noise ratio (SNR) at 1 kHz frequency, with an absolute value of capacitance variation significantly smaller for Dengue and Zika NS1 proteins ($|\Delta C| = 1.5 \pm 1.0$ nF and 1.8 ± 1.0 nF, respectively) than for the spike protein ($|\Delta C| = 7.0 \pm 1.8$ nF). Under the optimized conditions, the established biosensor is able to indicate that the sample contains target proteins when $|\Delta C| > 3.8$ nF, as determined by the cut-off value (CO). This immunosensor was developed using interdigitated electrodes which require a measurement system with a simple electrical circuit that can be miniaturized to enable point-of-care detection, offering an alternative for COVID-19 diagnosis, especially in areas where there is also a co-incidence of Zika and Dengue.

1. Introduction

Coronavirus disease 2019 (COVID-19) is a viral disease caused by the severe acute respiratory syndrome coronavirus 2 (SARS-CoV-2) that started in December 2019 and has rapidly spread worldwide, reaching >460 million cases and 6 million deaths by now (March 2022) [1]. Early detection of the disease has been the key to controlling its propagation and preventing further health, social, and economic damage. The main diagnostic methods consist of serological / antigen tests and molecular analyzes such as the RT-PCR (reverse transcription-polymerase chain reaction). At the beginning of the pandemic, the serological tests based on lateral-flow assay was widely used because it targets antibodies produced in response to the viral infection (immunoglobulin-M and immunoglobulin-G) in a rapid and low-cost way, being suitable for mass testing [2,3]. However, after the advent of anti-COVID-19 vaccines, this test is no longer considered appropriate because it could detect antibodies produced in response to the vaccine rather than the virus infection. The RT-PCR assay is the gold standard diagnostic method, as viral RNA can be detected in the early days of infection with high specificity and sensitivity, providing a reliable result. [4,5]. Other molecular tests are also being used, such as the loop-mediated isothermal amplification (LAMP), a modern and sensitive nucleic amplification method capable of recognizing up to eight sequences of the target gene in 1 h [6–8]. However, these methods are laborious, expensive, and require specialized professionals and laboratory infrastructure, making it difficult to attend to the growing demands. Currently, antigen tests using the lateral flow method are the most widely used for point-of-care diagnosis. They detect viral proteins within 15–20 min and provide a qualitative result [9]. Despite their low-cost and specificity, they are not as sensitive as molecular tests [9,10].

In addition to the COVID-19 pandemics, some tropical and subtropical countries are also facing epidemics of Dengue and Zika, viruses with similar symptoms in early stages and cross-reactivity with serological tests [11–14]. Misdiagnosis leads to a great concern with patient treatment as it can cause preventable fatalities, in addition to triggering outbreaks due to failures in the isolation of patients positive for COVID-19 and in vector control in the case of Dengue and Zika [15]. This scenario brings the crucial need for a simple, fast, specific, and low-cost

* Corresponding author.
E-mail address: isabellasampaio@ifsc.usp.br (I. Sampaio).
[1] Authors with equal contributions.

https://doi.org/10.1016/j.mee.2022.111912
Received 1 November 2022; Accepted 5 November 2022
Available online 9 November 2022

test, capable of distinguishing between SARS-CoV-2, Dengue virus (DenV), and Zika virus (ZikV) [13]. Biosensors are powerful tools for point-of-care diagnosis, being suitable for this specific situation [16–18]. Several biosensors have already been described for COVID-19, as shown in Table 1. However, they face some limitations and may fail to detect SARS-CoV-2 variants that have undergone point mutations in the Spike protein [19]. In addition, in epidemic and pandemic situations, when the demand for diagnostic tests can become very large, devices must be developed using different strategies to avoid a shortage of supplies needed for the fabrication of the tests. For example, when the daily cases of the omicron variant reached their peak, there was a high demand for lateral flow tests, and as a consequence, many countries stayed on alert over the possibility of a lack of the supplies -such as gold nanoparticles - which could limit production and availability of the diagnostic kits.

To offer a point-of-care diagnostic device, capacitive biosensors are interesting because they are easily miniaturized, user-friendly, and provide fast results [26,27]. Electrical capacitance-based biosensors measure the changes in the dielectric properties of specific electrodes when biorecognition events occur on their surface. Interdigitated electrodes are the most used for these devices and consist of several equally spaced metallic tracks, called fingers, with each pair acting as a planar capacitor [28]. They have been widely used for detecting different biomolecules, such as proteins [29–32], nucleic acids [33,34], and cells [35,36].

In this study, we describe a qualitative immunosensor based on the capacitive detection of spike proteins for COVID-19 diagnosis. The device can distinguish spike protein from Dengue and Zika NS1 proteins and, therefore, is suitable to be used in areas with co-incidence of these diseases. The use of polyclonal antibodies overcomes the detection troubles with mutations in the spike protein.

2. Material and methods

2.1. Materials

Cysteamine (C_2H_7NS, < 98%), N-hydroxisuccinimide ($C_4H_5NO_3$, NHS), 1-ethyl-3-(3-dimethylaminopropyl)carbodiimide ($C_8H_{17}N_3$, EDC), and bovine serum albumin (BSA) were purchased from Sigma-Aldrich (San Luis, Missouri, EUA). Chicken COVID-19 spike protein (S1 + S2 extracellular domain) coronavirus polyclonal antibody (MBS378285), COVID-19 spike protein coronavirus recombinant protein (MBS2563881), Zika Virus Antigen (MBS568704) and Dengue Virus NS1 Type 2 protein (MBS143474) were purchased from MyBioSource (San Diego, CA, USA). NaH_2PO_4, Na_2HPO_4, and NaCl used in the preparation of phosphate-buffered saline (PBS, pH 7.4, 10 mM) were also obtained from Sigma-Aldrich (San Luis, Missouri, EUA).

2.2. Fabrication of interdigitated electrodes (IDEs) and plasma cleaning

Gold interdigitated electrodes (IDEs) were fabricated using BK7 glass as the substrate for photolithography, followed by sputtering. To form an adhesion layer on the substrate, a 20 nm-thick chromium film was deposited. Then, it was covered with a gold layer of 120 nm-thick. Each electrode had 150 parallel metallic tracks (fingers) with a 10 μm gap between them, in which each pair works as a planar capacitor. The electrodes were cleaned with oxygen plasma to remove organic residues, using Tergeo Plasma Cleaner equipment under the following conditions: medium O_2, 35 W power, and a gas flow rate of 5 sccm (cm^3/min).

2.3. Antibody immobilization

To obtain a more sensitive detection, two methods were tested for the construction of the self-assembled monolayers: In the first method, immobilization of the antibodies was carried out by electrostatic interaction, and in the second method, the antibodies were immobilized by covalent bonding (Fig. 1). For the electrostatic immobilization, the IDEs were incubated overnight (15 h) with cysteamine 10 mM (a 100 mM stock solution was prepared in ethanol and then diluted in ultrapure water). A solution containing 250 μg/mL of anti-Spike antibodies was added to the modified electrodes and left to interact for 3 h. To block the remaining active sites, the IDEs were incubated with a 1% BSA solution in PBS buffer (10 mM, pH 7.4, 0.1 M NaCl) for 30 min.

For the covalent immobilization, a mixture containing EDC/NHS (8 mM/5 mM) and antibodies (4 μg/mL or 40 μg/mL) was prepared in PBS buffer and incubated for 2 h at 4 °C to activate the carboxylic groups in the antibodies (H^+ deprotonation). Immobilization was performed by adding the mixture containing the activated antibodies to the IDEs modified with cysteamine. In this case, the carboxylic groups of the antibodies covalently bond to the amine group of the cysteamine on the electrode surface. The blocking step was also performed. All incubation steps were performed at 4 °C and to remove non-bounded molecules, the IDEs were subsequently immersed in 10 mM PBS and ultrapure water. Finally, the electrodes were carefully dried in N_2 flow.

2.4. Characterization of electrodes surface

To determine the roughness of the IDEs after each modification step, atomic force microscopy (AFM) was used. The images were collected in tapping mode using a NanoSurf Flexa microscope (Nanosurf, Switzerland) and a cantilever with a resonant frequency of 300 kHz and a spring constant of 40 N/m. The IDEs were also analyzed by Raman spectroscopy to assess whether the molecules were successfully immobilized on their surface by identifying their characteristic functional groups. Raman spectra were collected in an inVia™ Raman confocal microscope (Renishaw, UK) with a 532 nm laser (power of 5%) using a 50× objective and a grating of 1800 lines/mm. Single spectrum measurements were recorded in the 500–3800 cm^{-1} range, with 10 s acquisition and 20 accumulations. Raman mapping was conducted by collecting the spectra in the 840–2470 cm^{-1} range with 30 s acquisition and 3 accumulations at each point. The mapped area (x = 88 μm and y = 12 μm) contains 315 data points (2 m of step size). Images were generated by mapping the intensity of the band related to the amide bond (1570 cm^{-1}) in each spectrum. All data handling and processing, as well as 2D and 3D color map reconstructions, were proceeded in WiRE 5.4 software.

2.5. Target proteins detection

Functionalized IDEs were incubated for 30 min with 10 μL of Spike

Table 1
Comparison of different biosensors for SARS-CoV-2 detection.

Method	Target	Sample	Limit of detection	Time	Reference
Plasmonic	IgG	Blood	Not mentioned	30 min	[20]
Electrochemical	microRNA	Synthetic sequences	10 pM	1 h	[21]
Surface-enhanced Raman scattering (SERS)	Spike protein	Untreated saliva	6 fg/mL	4 h	[22]
Field-effect transistor (FET)	Spike protein	Nasopharyngeal swab	100 fg/mL	1 h	[23]
Electrochemical	IgG / IgM	Sera	1 ng/mL	30 min	[24]
Capacitive	Nucleoprotein	Viral cultures	4.1 ng/mL	1 h	[25]

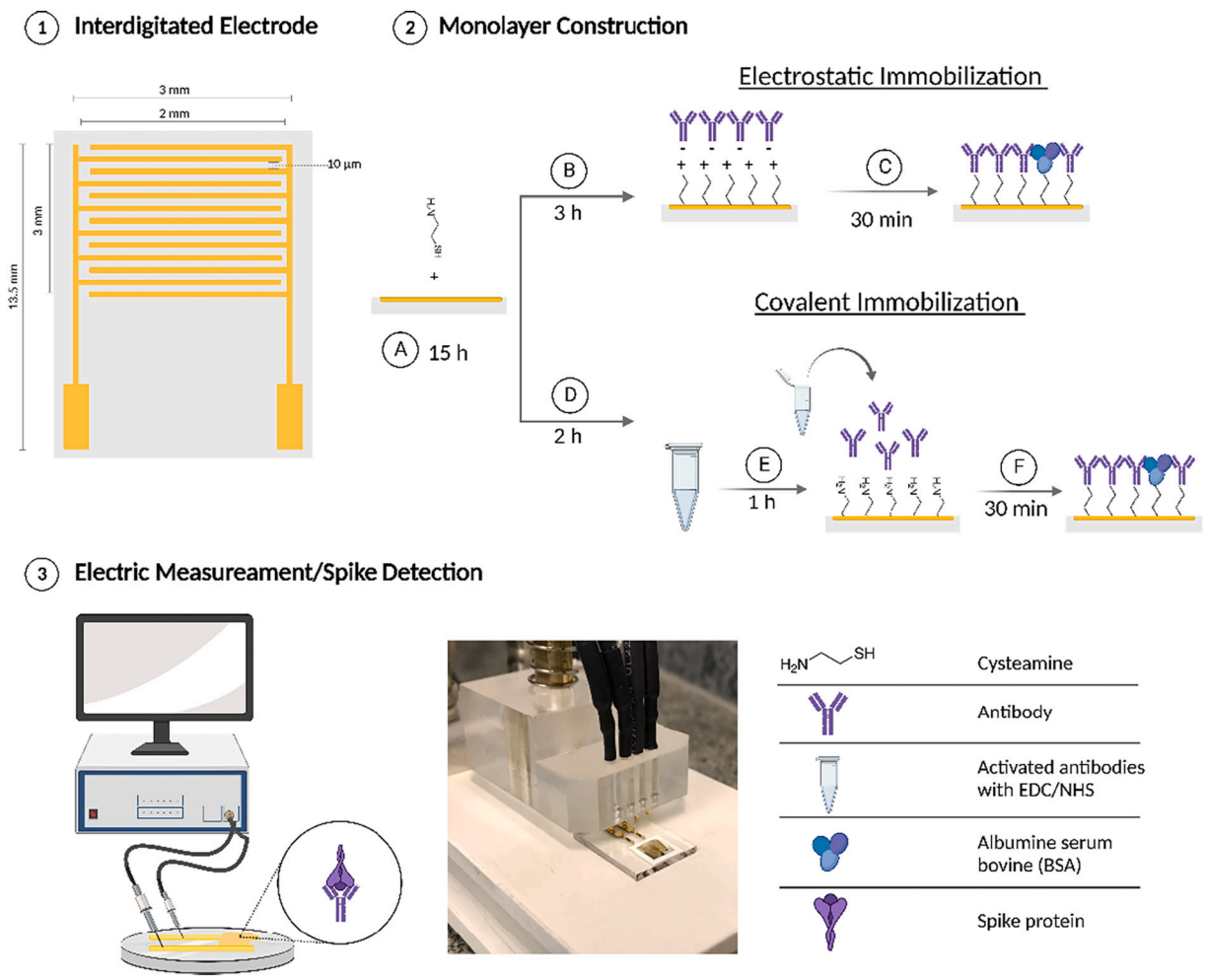

Fig. 1. Experimental setup. 1) Monolayer construction – A) Cysteamine 10 mM incubation. B) Electrostatic immobilization of antibodies. C) Blocking active sites with BSA 1%. D) Pre-activating antibodies with EDC/NHS for 2 h. E) Covalent immobilization of antibodies by carboxyl groups bound to amine groups from cysteamine. F) Blocking active sites with BSA 1%. 2) Spike protein detection.

protein 2.5 µg/mL in 10 mM PBS buffer (positive sample). This protein concentration was chosen based on the clinical range reported in a previous study [37]. Following, the IDEs were washed and dried. After this step, the electrodes were submitted to the electrical capacitance measurements. Selectivity analyses were carried out with negative controls, using the NS1 protein of both Dengue and Zika Viruses, in the same concentration and conditions as the positive protein. The selectivity tests were performed in 6 independent electrodes ($n = 6$) for each sample to evaluate the reproducibility of the results.

2.6. Electrical capacitance measurements

Electrical capacitance measurements were performed in 10 µL of 10 mM PBS buffer, at room temperature, and an incubation time of 10 min for the electrical double layer to be organized. The spectra were collected in the frequency range of 100 Hz to 1 MHz using a Solartron Analytical 1260A (Ametek) with SMaRT Impedance Measurement software.

2.7. Statistical analyses

The statistical analyses of the capacitance data were performed using the one-way analysis of variance (ANOVA) with the Tukey posthoc test and Student's *t*-test to determine whether differences between sample groups are statistically relevant. An alpha of 0.05 was used and $p < 0.05$ was considered significant.

3. Results and discussion

3.1. Characterization of SAMs on IDEs surface

The roughness of the IDEs for each step of the SAMs construction was evaluated by AFM (Fig. 2). For bare electrodes, the average roughness was 0.9 ± 0.1 nm (Fig. 2a), which increased to 1.6 ± 0.2 nm after incubation with cysteamine (Fig. 2b), indicating that these molecules bonded to the IDEs surface. For the electrostatic immobilization method, the roughness after incubation with the antibody (Fig. 2c) was 1.7 ± 0.2 nm. The small variation in surface roughness points to the low efficiency of this strategy in the immobilization of antibodies and proteins.

For covalent immobilization, two antibody concentrations were tested. The average roughness of the electrodes after incubation with 4 µg/mL of antibodies was 1.4 ± 0.2 nm (Fig. 4d) while for the incubation with 40 µg/mL, the roughness was 3.0 ± 0.5 nm (Fig. 4e). Comparing these results with the value found for IDEs modified only with cysteamine (1.6 ± 0.2 nm, Fig. 4b) one may be observed that immobilization with 4 µg/mL did not change the electrode roughness, indicating that this concentration can be too low for the construction of the SAM. However, incubation with 40 µg/mL of antibodies produced a significant increase in roughness, which can be due to the successful immobilization of antibodies on the electrode surface. The AFM analyses show

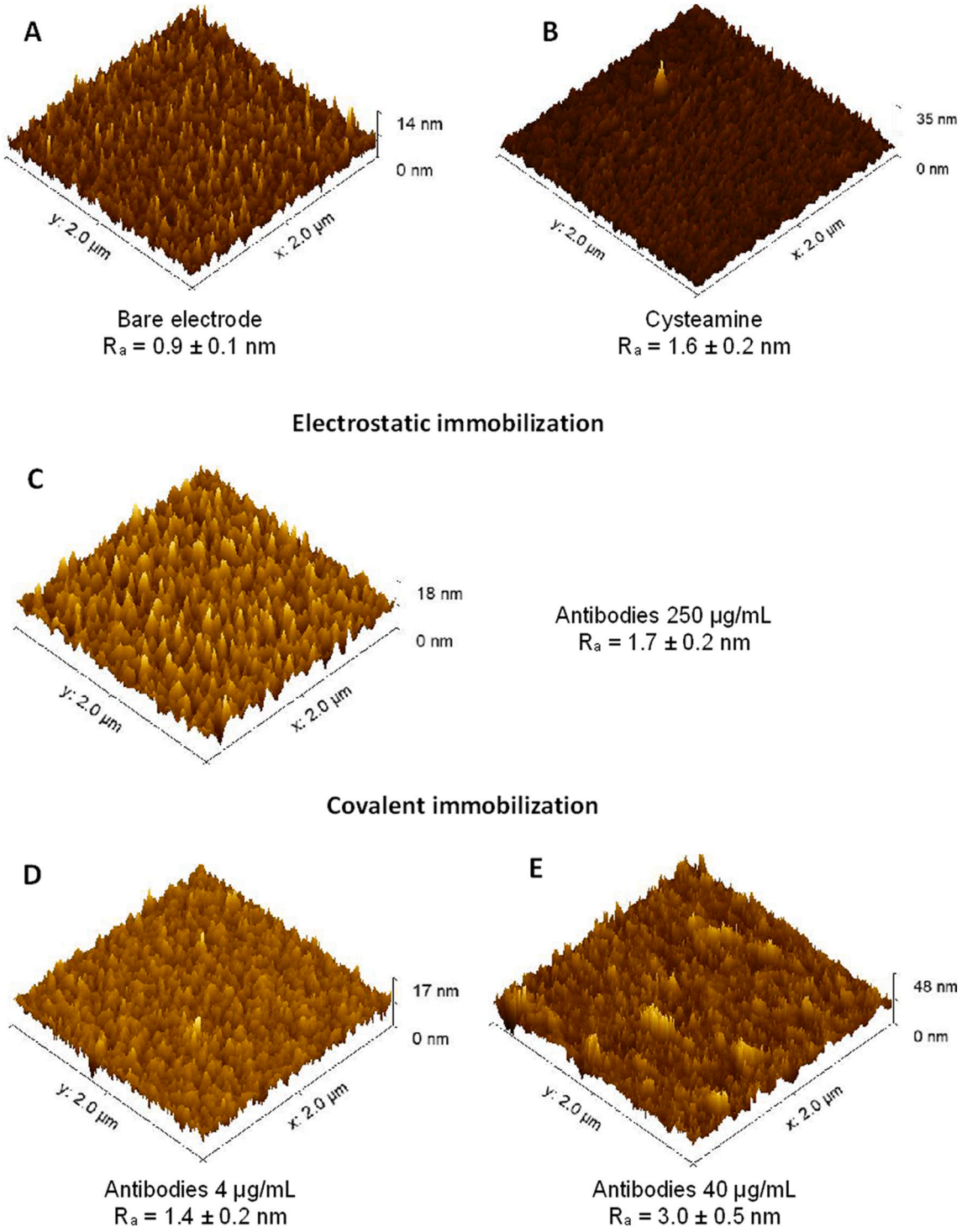

Fig. 2. AFM images of the SAM construction steps: (a) Bare electrode. (b) After 10 mM cysteamine deposition. (c) Electrostatic immobilization of antibody 250 µg/mL. (d) Covalent immobilization of activated antibody 4 µg/mL. (e) Covalent immobilization of activated antibody 40 µg/mL. The images were collected in tapping mode with 512 pixels resolution in 2 µm × 2 µm.

that for the construction of the SAMs, the covalent immobilization of antibodies at a concentration of 40 µg/mL was more efficient, since roughness is expected to increase when antibodies are immobilized on a smooth surface, such as cysteamine-modified IDEs.

The SAM construction steps were also characterized by Raman spectroscopy to identify the functional groups of the immobilized molecules. Fig. 3 shows the spectra collected for the electrodes modified by the covalent immobilization method. The bands at 520 cm^{-1} and 1250 cm^{-1} observed in all spectra come from the vibrational modes of crystalline Si on the BK7 glass substrate. After incubation with cysteamine, two new peaks are observed, at 1480 cm^{-1} referring to the CH_2 group and at 1520 cm^{-1} attributed to the NH_2 vibrational mode, which are characteristic of this molecule. The latter indicates the cysteamine immobilization onto IDEs, possibly by the interaction between the thiol group of cysteamine and the gold surface. In the spectra collected after the antibodies immobilization, peaks at 1406 cm^{-1} and 1560 cm^{-1} are

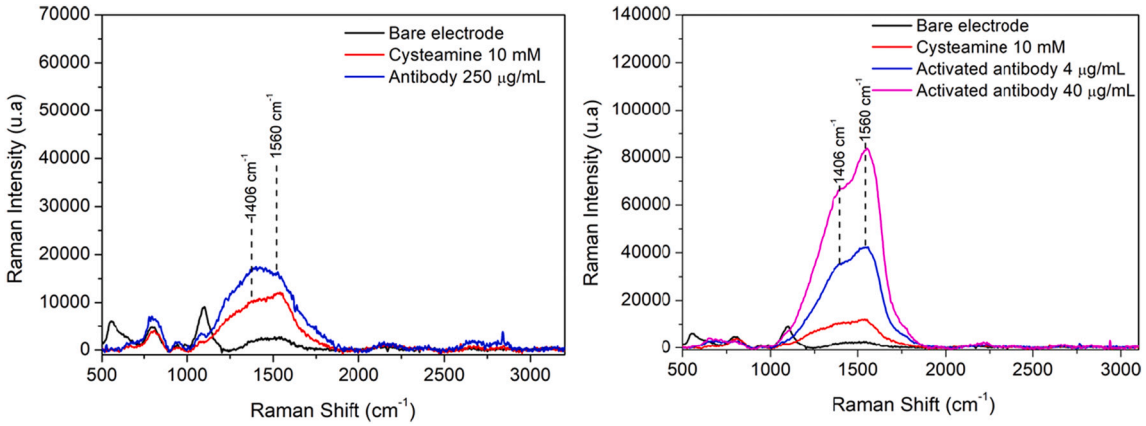

Fig. 3. Raman spectra of the SAMs construction steps of (a) the electrostatic immobilization and (b) the covalent immobilization of antibodies at two different concentrations, 4 and 40 µg/mL. Spectra were collected using a 532 nm laser, in the frequency range from 100 to 3500 cm^{-1} and 10 accumulations with an acquisition time of 30 s each.

observed, which are characteristic of the C═N vibration coming from the amide bond between activated carboxylic groups from antibody and amine group from cysteamine. The latter reveals that the covalent bond between the amine group of cysteamine and the carboxylic group of the antibody occurred. Furthermore, comparing the spectra obtained for the two antibody concentrations, we can observe that the intensity of the peaks is greater for the modified electrode with the highest concentration of antibodies. Corroborating the AFM analyses, the Raman spectra indicate that the construction of the SAMs with the covalent immobilization of antibodies at a concentration of 40 µg/mL is efficient, and therefore it was chosen for the other tests.

Raman mapping was conducted to identify the spatial distribution of the immobilized antibodies onto the Au fingers of the IDE. Fig. 4a shows an optical micrograph for the IDE with the covalent immobilization of antibodies at 40 µg/mL. Structures in the form of small islands along the surfaces are observed, with sizes falling into the 0.5–3.5 µm range. The mapping was conducted by monitoring the intensity of the peak at 1560 cm^{-1} assigned to amide bonds inside the area demarked by the white dashed rectangle. Fig. 4b and c show the resulting 2D and 3D reconstructions, respectively, obtained by the aforementioned procedure. The highest intensities for the amide bonds coincide with the concentrated deposits, as evidenced by the regions with yellowish-white colors in both 2D and 3D Raman maps. Hence, the results of the color distributions indicate that the islands along the IDE are composed of the deposited antibodies.

3.2. *Capacitive measurements*

The biosensor construction steps were monitored by capacitance measurements. As shown in Fig. 5, the capacitance after modification with cysteamine dropped sharply for the frequency range 10^2–10^4 Hz, which can be attributed to the change in the dielectric properties of the IDEs caused by the positively charged amine groups. This indicates that the gold surface functionalization with cysteamine was successful. Immobilization of the antibodies produced a subtle change in capacitance (inset of Fig. 5), possibly due to the low concentration used. To

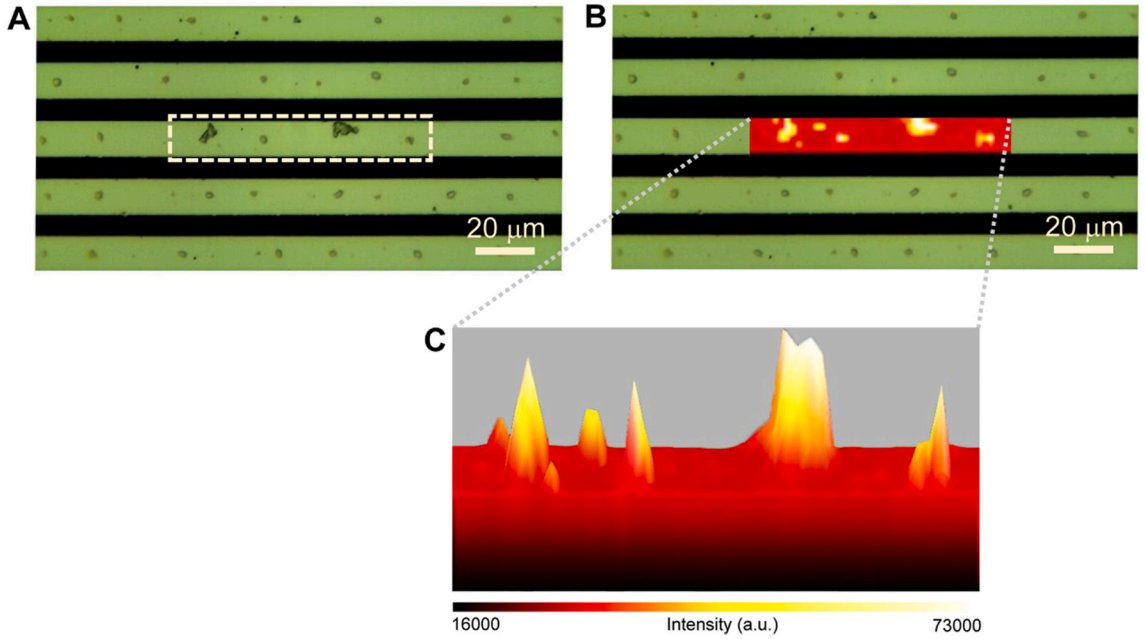

Fig. 4. Raman mapping of the IDEs containing the covalently anti-SARS-Cov-2 immobilized antibodies at 40 µg/mL: (a) Optical micrograph showing a magnified view of the IDE and the region selected for the analysis (white dashed rectangle). (b,c) 2D and 3D Raman intensity mapping, respectively, showing the peaks from the amide vibrational mode at 1560 cm^{-1}.

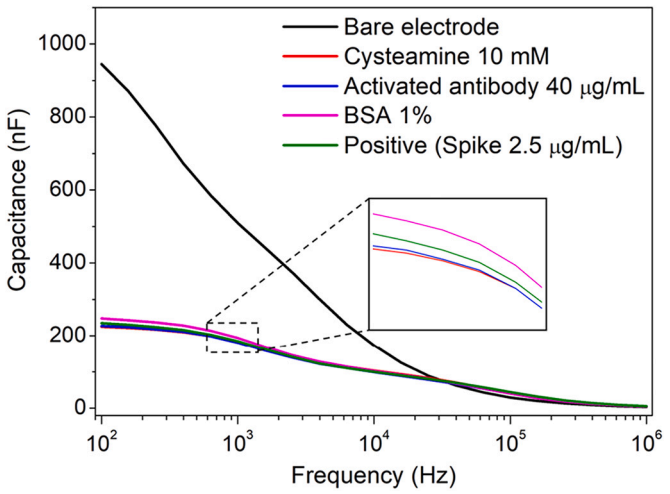

Fig. 5. Capacitance curves after each step of biosensor construction and detection of the target protein (spike 2.5 μg/mL) in the frequency range of 10^2–10^6 Hz. The zoomed-in view shows the spectra in the low-frequency region.

avoid unspecific interactions, the surface was blocked with 1% BSA and a dramatic increase in the capacitance was observed, possibly due to the negative charges of the proteins that increase the density of counter-ions and the capacitance. After the blocking step, the detection of the target protein in a clinically relevant concentration was tested. A decrease in the capacitance value was observed after interaction with the spike protein, indicating that the biosensor was able to detect it. As the capacitance is measured between the electrode and counter-ions layer and is inversely proportional to the distance between them, the capacitance decrease after the antigen-antibody binding can be attributed to the additional layer formed by the spike proteins, which displaces the counter-ion layer [38–40]. The spectra also reveal that for this device, the sample analysis should be performed at low frequencies (10^2–10^3 Hz), where the electrical properties of the electrodes seem to be more sensitive to the events occurring on their surface.

To evaluate the biosensor performance and also to choose the best frequency for the selectivity tests, 5 consecutive measurements were performed on one electrode after the blocking step of the SAM construction. Fig. 6A shows the great repeatability of the biosensor over the entire frequency range. For the fixed frequency of 10^3 Hz, the average capacitance value of the 5 measurements was (185.2 ± 0.5) nF, showing an excellent relative standard deviation (RSD) of 0.24%. We observed that after the second measurement, the biosensor stabilizes and no significant change in capacitance is noticed (Fig. 6B). This is important to ensure that changes in capacitance obtained after interaction with the target molecule are due to specific antigen-antibody binding.

The biosensor selectivity was evaluated by performing capacitance measurements before and after incubation with negative samples (NS1 DenV and NS1 ZikV) under the same conditions as the tests with positive samples. The biosensor response was evaluated as the absolute value of the capacitance variation ($|\Delta C| = C_{after} - C_{before}$) in 6 independent electrodes ($n = 6$) from each of the sample groups. As shown in Fig. 7A, the biosensor response for the two negative groups was similar, the $|\Delta C|$ values obtained were 1.5 ± 1.0 nF and 1.8 ± 1.0 nF for NS1 proteins from ZikV and DenV, respectively. The difference in the means is not statistically relevant at the 0.05 level ($p > 0.05$). More importantly, the capacitance variation for both was significantly smaller than for the positive group ($|\Delta C| = 7.0 \pm 1.8$ nF), and the relevant difference ($p < 0.001$) demonstrates that the biosensor selectively recognizes the spike protein. The signal-to-noise ratio (SNR) was calculated considering the $|\Delta C|$ for spike protein as the signal and the $|\Delta C|$ for the NS1 proteins as the noise. The SNR obtained for DenV was 3.9 ± 2.8 and for ZikV was 4.7 ± 1.7, which are good values compared to those presented by other biosensors [41,42]. Based on a 95% confidence interval, the cut-off value (CO) was determined to be 3.8 nF. It was calculated as $CO = \bar{x} + 1.96$ x SD, where $\bar{x}$ is the average of the $|\Delta C|$ for the samples containing the NS1 DenV. Therefore, when the biosensor presents a $|\Delta C| >$ 3.8 nF, it indicates that the sample contains the spike protein from the SARS-CoV-2 virus.

4. Conclusion

We have reported a qualitative biosensor for the electrical detection of the spike protein from the SARS-CoV-2 virus. To overcome the limitations caused by mutations in the target protein, the biorecognition layer is formed by polyclonal antibodies. Based on the absolute value of the capacitive variation, we demonstrated the selectivity of the biosensor against the NS1 proteins of ZikV and DenV, which are viral diseases with symptoms similar to those of COVID-19. Therefore, this device is suitable to be used in regions where these diseases are coincident. The capacitive biosensor uses a simple and low-cost methodology in addition to providing fast results. For biomarkers that are present in the virus, such as the spike protein of the SARS-CoV-2, qualitative analysis is sufficient to detect viral infection and, therefore, can be used for the screening of infected people. In addition, the interdigitated electrodes used in this biosensor require a measurement system with a simple electrical circuit that can be miniaturized to enable point-of-care detection, offering an alternative to current diagnostic methods for COVID-19.

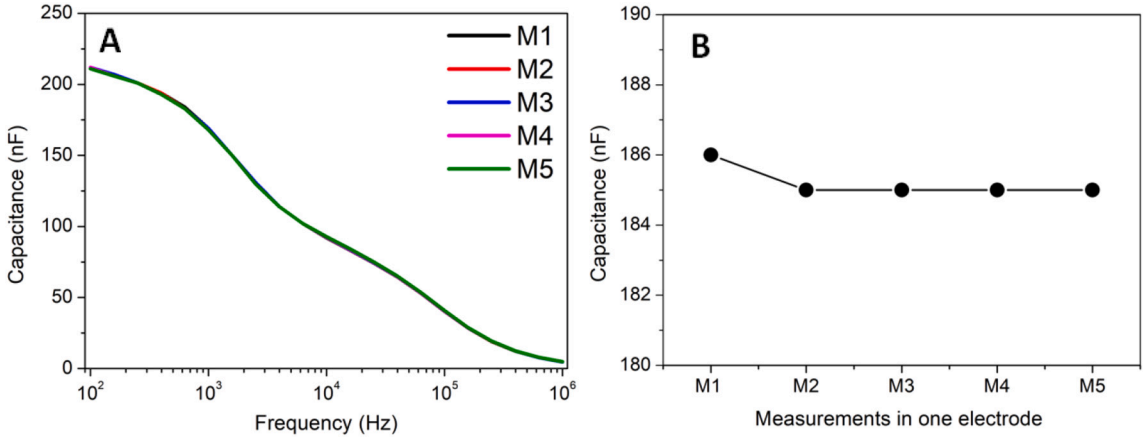

Fig. 6. Repeatability tests. (A) Capacitance curves of 5 consecutive measurements (M1 - M5) on the same electrode after SAM construction in the frequency range of 10^2–10^6 Hz. (B) Capacitance values of the consecutive measurements for the fixed frequency at 10^3 Hz.

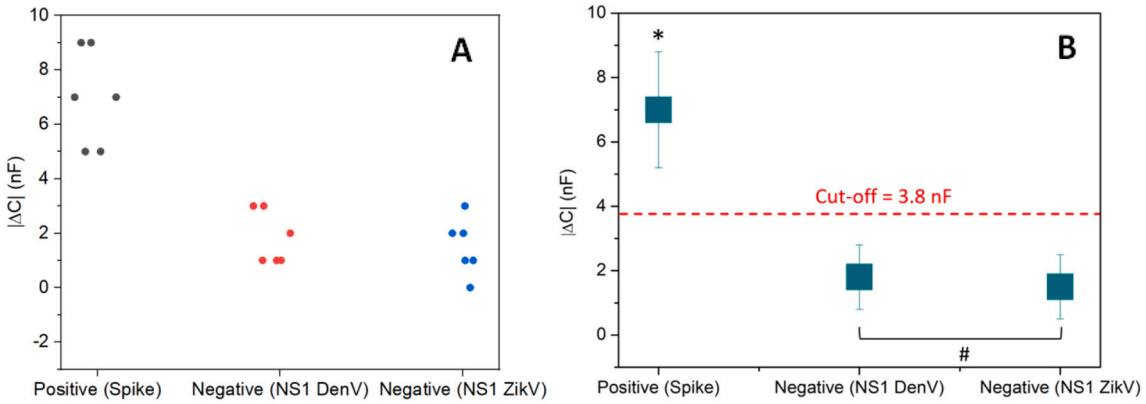

Fig. 7. Biosensor selectivity: (a) Dot plot of positive (Spike protein) and negative samples (NS1 DenV and NS1 ZikV) at a concentration of 2.5 μg/mL. The average value and standard deviation of |ΔC| were determined from 6 independent electrodes for each group ($n = 6$). (b) Box plot showing the cut-off at 3.8 nF (dashed line) based on a 95% confidence interval. *Statistically different from negative groups ($p < 0.001$), #The difference in the means is not statistically relevant at the 0.05 level ($p > 0.05$).

CRediT authorship contribution statement

Isabella Sampaio: Conceptualization, Methodology, Formal analysis, Writing – original draft, Writing – review & editing. **Nayla Naomi Kusimoto Takeuti:** Conceptualization, Methodology, Formal analysis, Writing – original draft, Writing – review & editing. **Beatriz Gusson:** Methodology, Formal analysis, Writing – review & editing. **Thales Rafael Machado:** Methodology, Formal analysis, Writing – review & editing. **Valtencir Zucolotto:** Writing – review & editing, Funding acquisition, Supervision.

Declaration of Competing Interest

The authors declare that they have no known competing financial interests or personal relationships that could have appeared to influence the work reported in this paper.

Data availability

Data will be made available on request.

Acknowledgements

The authors gratefully acknowledge the financial support provided by the National Council for Scientific and Technological Development - CNPq (Grant numbers 88887.514079/2020, 382078/2020-9, 164373/2020-9, 440496/2016-0), Coordination of Superior Level Staff Improvement (CAPES) (88881.130763/2016-01) and São Paulo Research Foundation - FAPESP (Grant number 2020/03015-2). We are also grateful for the cooperation of the researchers from the Nanomedicine and Nanotoxicology Group in our studies.

References

[1] World Health Organization, Coronavirus Disease 2019 (COVID-19) - Situation Report 72, 2020, https://doi.org/10.1001/jama.2020.2633.
[2] P. Khan, L.M. Aufdembrink, A.E. Engelhart, Isothermal SARS-CoV-2 diagnostics: tools for enabling distributed pandemic testing as a means of supporting safe reopenings, ACS Synth. Biol. 9 (2020) 2861–2880, https://doi.org/10.1021/acssynbio.0c00359.
[3] R.W. Peeling, C.J. Wedderburn, P.J. Garcia, D. Boeras, N. Fongwen, J. Nkengasong, A. Sall, A. Tanuri, D.L. Heymann, Serology testing in the COVID-19 pandemic response, Lancet Infect. Dis. 20 (2020) e245–e249, https://doi.org/10.1016/S1473-3099(20)30517-X.
[4] M. Shen, Y. Zhou, J. Ye, A.A. Abdullah AL-Maskri, Y. Kang, S. Zeng, S. Cai, Recent advances and perspectives of nucleic acid detection for coronavirus, J. Pharm. Anal. 10 (2020) 97–101, https://doi.org/10.1016/j.jpha.2020.02.010.
[5] N. Gupta, S. Augustine, T. Narayan, A. O'Riordan, A. Das, D. Kumar, J.H.T. Luong, B.D. Malhotra, Point-of-care PCR assays for COVID-19 detection, Biosensors. 11 (2021), https://doi.org/10.3390/bios11050141.
[6] C. Yan, J. Cui, L. Huang, B. Du, L. Chen, G. Xue, S. Li, W. Zhang, L. Zhao, Y. Sun, H. Yao, N. Li, H. Zhao, Y. Feng, S. Liu, Q. Zhang, D. Liu, J. Yuan, Rapid and visual detection of 2019 novel coronavirus (SARS-CoV-2) by a reverse transcription loop-mediated isothermal amplification assay, Clin. Microbiol. Infect. 26 (2020) 773–779, https://doi.org/10.1016/j.cmi.2020.04.001.
[7] L.E. Lamb, S.N. Bartolone, E. Ward, M.B. Chancellor, Rapid detection of novel coronavirus (COVID19) by reverse transcription-loop-mediated isothermal amplification, Lancet. (2020), https://doi.org/10.2139/ssrn.3539654.
[8] W. Yang, X. Danga, Q. Wang, M. Xu, Rapid detection of SARS-CoV-2 using reverse transcription RT-LAMP method, MedRxiv. (2020) 4–5, https://doi.org/10.1101/2020.03.02.20030130.
[9] R.W. Peeling, P.L. Olliaro, D.I. Boeras, N. Fongwen, Scaling up COVID-19 rapid antigen tests: promises and challenges, Lancet Infect. Dis. 21 (2021) e290–e295, https://doi.org/10.1016/S1473-3099(21)00048-7.
[10] A. Scohy, A. Anantharajah, M. Bodéus, B. Kabamba-Mukadi, A. Verroken, H. Rodriguez-Villalobos, Low performance of rapid antigen detection test as frontline testing for COVID-19 diagnosis, J. Clin. Virol. 129 (2020), 104455, https://doi.org/10.1016/j.jcv.2020.104455.
[11] Y. Lustig, S. Keler, R. Kolodny, N. Ben-Tal, D. Atias-Varon, E. Shlush, M. Gerlic, A. Munitz, R. Doolman, K. Asraf, L.I. Shlush, A. Vivante, Potential antigenic cross-reactivity between severe acute respiratory syndrome coronavirus 2 (SARS-CoV-2) and dengue viruses, Clin. Infect. Dis. 73 (2021) e2444–e2449, https://doi.org/10.1093/cid/ciaa1207.
[12] M.S. Santoso, S. Masyeni, S. Haryanto, B. Yohan, M.L. Hibberd, R.T. Sasmono, Assessment of dengue and COVID-19 antibody rapid diagnostic tests cross-reactivity in Indonesia, Virol. J. 18 (2021) 1–5, https://doi.org/10.1186/s12985-021-01522-2.
[13] S.Q. Khairunisa, I.H. Amarullah, S. Churrotin, A.L. Fitria, M. Amin, M.I. Lusida, S. Soegijanto, Potential misdiagnosis between COVID-19 and dengue infection using rapid serological test, Infect. Dis. Rep. 13 (2021) 540–551, https://doi.org/10.3390/idr13020050.
[14] D. Lokida, N. Lukman, G. Salim, D.P.B. Butar, H. Kosasih, W.N. Wulan, A. M. Naysilla, Y. Djajady, R.A. Sari, D. Arlinda, C.Y. Lau, M. Karyana, Diagnosis of COVID-19 in a dengue-endemic area, Am. J. Trop. Med. Hyg. 103 (2020) 1220–1222, https://doi.org/10.4269/ajtmh.20-0676.
[15] A. Wilder-Smith, H. Tissera, E.E. Ooi, J. Coloma, T.W. Scott, D.J. Gubler, Preventing dengue epidemics during the COVID-19 pandemic, Am. J. Trop. Med. Hyg. 103 (2020) 570–571, https://doi.org/10.4269/ajtmh.20-0480.
[16] A. Rodrigues, I. Sampaio, E. Jos, N. Cristi, S. Vieira, V. Zucolotto, Detecting cancer cells with a highly sensitive LbL-based biosensor, Talanta. 233 (2021), https://doi.org/10.1016/j.talanta.2021.122506.
[17] H.A.M. Faria, V. Zucolotto, Label-free electrochemical DNA biosensor for zika virus identification, Biosens. Bioelectron. 131 (2019) 149–155, https://doi.org/10.1016/j.bios.2019.02.018.
[18] A. Figueiredo, N.C.S. Vieira, J.F.D. Santos, B.C. Janegitz, S.M. Aoki, P.P. Junior, R. L. Lovato, M.L. Nogueira, V. Zucolotto, F.E.G. Guimarães, Electrical detection of dengue biomarker using egg yolk immunoglobulin as the biological recognition element, Sci. Rep. 7 (2017) 46865, https://doi.org/10.1038/srep46865.
[19] H. Xi, H. Jiang, M. Juhas, Y. Zhang, Multiplex biosensing for simultaneous detection of mutations in SARS-CoV-2, ACS Omega. 6 (2021) 25846–25859, https://doi.org/10.1021/acsomega.1c04024.
[20] N.C. Cady, N. Tokranova, A. Minor, N. Nikvand, K. Strle, W.T. Lee, W. Page, E. Guignon, A. Pilar, G.N. Gibson, Multiplexed detection and quantification of human antibody response to COVID-19 infection using a plasmon enhanced biosensor platform, Biosens. Bioelectron. 171 (2021), 112679, https://doi.org/10.1016/j.bios.2020.112679.

[21] S.N. Pang, Y.L. Lin, K.J. Yu, Y.E. Chiou, W.H. Leung, W.H. Weng, An effective sars-cov-2 electrochemical biosensor with modifiable dual probes using a modified screen-printed carbon electrode, Micromachines. 12 (2021), https://doi.org/10.3390/mi12101171.

[22] M. Zhang, X. Li, J. Pan, Y. Zhang, L. Zhang, C. Wang, X. Yan, X. Liu, G. Lu, Ultrasensitive detection of SARS-CoV-2 spike protein in untreated saliva using SERS-based biosensor, Biosens. Bioelectron. 190 (2021), 113421, https://doi.org/10.1016/j.bios.2021.113421.

[23] G. Seo, G. Lee, M.J. Kim, S.H. Baek, M. Choi, K.B. Ku, C.S. Lee, S. Jun, D. Park, H. G. Kim, S.J. Kim, J.O. Lee, B.T. Kim, E.C. Park, S. Il Kim, Rapid detection of COVID-19 causative virus (SARS-CoV-2) in human nasopharyngeal swab specimens using field-effect transistor-based biosensor, ACS Nano 14 (2020) 5135–5142, https://doi.org/10.1021/acsnano.0c02823.

[24] A. Yakoh, U. Pimpitak, S. Rengpipat, N. Hirankarn, O. Chailapakul, S. Chaiyo, Paper-based electrochemical biosensor for diagnosing COVID-19: detection of SARS-CoV-2 antibodies and antigen, Biosens. Bioelectron. 176 (2021), 112912, https://doi.org/10.1016/j.bios.2020.112912.

[25] J.H. Park, G.Y. Lee, Z. Song, J.H. Bong, Y.W. Chang, S. Cho, M.J. Kang, J.C. Pyun, Capacitive biosensor based on vertically paired electrodes for the detection of SARS-CoV-2, Biosens. Bioelectron. 202 (2022), 113975, https://doi.org/10.1016/j.bios.2022.113975.

[26] G. Ertürk, B. Mattiasson, Capacitive biosensors and molecularly imprinted electrodes, Sensors (Switzerland). 17 (2017) 1–21, https://doi.org/10.3390/s17020390.

[27] B. Mattiasson, M. Hedström, Capacitive biosensors for ultra-sensitive assays, TrAC - Trends Anal. Chem. 79 (2016) 233–238, https://doi.org/10.1016/j.trac.2015.10.016.

[28] C. Berggren, B. Bjarnason, G. Johansson, Capacitive biosensors, Electroanalysis. 13 (2001) 173–180, https://doi.org/10.1002/1521-4109(200103)13:3<173::AID-ELAN173>3.0.CO;2-B.

[29] M. Labib, M. Hedström, M. Amin, B. Mattiasson, A capacitive immunosensor for detection of cholera toxin, Anal. Chim. Acta 634 (2009) 255–261, https://doi.org/10.1016/j.aca.2008.12.035.

[30] A. Foubert, N.V. Beloglazova, M. Hedström, S. De Saeger, Antibody immobilization strategy for the development of a capacitive immunosensor detecting zearalenone, Talanta. 191 (2019) 202–208, https://doi.org/10.1016/j.talanta.2018.08.062.

[31] Â.C. Perinoto, R.M. Maki, M.C. Colhone, F.R. Santos, V. Migliaccio, K. R. Daghastanli, R.G. Stabeli, P. Ciancaglini, F.V. Paulovich, M.C.F. De Oliveira, O. N. Oliveira, V. Zucolotto, Biosensors for efficient diagnosis of leishmaniasis: innovations in bioanalytics for a neglected disease, Anal. Chem. 82 (2010) 9763–9768, https://doi.org/10.1021/ac101920t.

[32] V. Zucolotto, K.R.P. Daghastanli, C.O. Hayasaka, A. Riul, P. Ciancaglini, O. N. Oliveira, Using capacitance measurements as the detection method in antigen-containing layer-by-layer films for biosensing, Anal. Chem. 79 (2007) 2163–2167, https://doi.org/10.1021/ac0616153.

[33] L. Wang, M. Veselinovic, L. Yang, B.J. Geiss, D.S. Dandy, T. Chen, A sensitive DNA capacitive biosensor using interdigitated electrodes, Biosens. Bioelectron. 87 (2017) 646–653, https://doi.org/10.1016/j.bios.2016.09.006.

[34] C. Cheng, R. Oueslati, J. Wu, J. Chen, S. Eda, Capacitive DNA sensor for rapid and sensitive detection of whole genome human herpesvirus-1 dsDNA in serum, Electrophoresis. 38 (2017) 1617–1623, https://doi.org/10.1002/elps.201700043.

[35] J. Jantra, P. Kanatharana, P. Asawatreratanakul, M. Hedstrom, B. Mattiasson, P. Thavarungkul, Real-time label-free affinity biosensors for enumeration of total bacteria based on immobilized concanavalin A, J. Environ. Sci. Heal. - Part A Toxic/Hazardous Subst. Environ. Eng. 46 (2011) 1450–1460, https://doi.org/10.1080/10934529.2011.609022.

[36] A. Qureshi, A. Pandey, R.S. Chouhan, Y. Gurbuz, J.H. Niazi, Whole-cell based label-free capacitive biosensor for rapid nanosize-dependent toxicity detection, Biosens. Bioelectron. 67 (2015) 100–106, https://doi.org/10.1016/j.bios.2014.07.038.

[37] A. Idili, C. Parolo, R. Alvarez-Diduk, A. Merkoçi, Rapid and efficient detection of the SARS-CoV-2 spike protein using an electrochemical aptamer-based sensor, ACS Sensors. 6 (2021) 3093–3101, https://doi.org/10.1021/acssensors.1c01222.

[38] A. Georgas, E. Lampas, D.P. Houhoula, A. Skoufias, S. Patsilinakos, I. Tsafaridis, G. P. Patrinos, N. Adamopoulos, A. Ferraro, E. Hristoforou, ACE2-based capacitance sensor for rapid native SARS-CoV-2 detection in biological fluids and its correlation with real-time PCR, Biosens. Bioelectron. 202 (2022), 114021, https://doi.org/10.1016/j.bios.2022.114021.

[39] K. Teeparuksapun, M. Hedström, B. Mattiasson, A sensitive capacitive biosensor for protein a detection using human igg immobilized on an electrode using layer-by-layer applied gold nanoparticles, Sensors. 22 (2022), https://doi.org/10.3390/s22010099.

[40] C. Berggren, G. Johansson, Capacitance measurements of antibody-antigen interactions in a flow system, Anal. Chem. 69 (1997) 3651–3657, https://doi.org/10.1021/ac970203e.

[41] J. Liu, L. Quan, X. Yu, L. Wang, Quantitative detection of procalcitonin using an electrochemical immunosensor based on MoO3/au@rGO nanocomposites, Analyst. 144 (2019) 6968–6974, https://doi.org/10.1039/c9an01721f.

[42] S. Wu, J. Hao, S. Yang, Y. Sun, Y. Wang, W. Zhang, H. Mao, X.M. Song, Layer-by-layer self-assembly film of PEI-reduced graphene oxide composites and cholesterol oxidase for ultrasensitive cholesterol biosensing, Sensors Actuators B Chem. 298 (2019), 126856, https://doi.org/10.1016/j.snb.2019.126856.